Nematic to Smectic-A Phase Transition under Shear Flow: A Nonequilibrium Synchrotron X-Ray Study

C. R. Safinya, E. B. Sirota, and R. J. Plano
Exxon Research and Engineering Company, Annandale, New Jersey 08801
(Received 3 December 1990)

We report on x-ray scattering studies of the nematic to smectic-A transition in 4-cyano-4′-octylbiphenyl under nonequilibrium shear-flow conditions. As the transition is approached, the interplay between the viscous frictional and the *flow-induced-fluctuation* forces on the nematic director leads to a series of regimes whose occurrence results from the divergence in one of the viscosities due to the critical slowing down of the smectic-A order-parameter fluctuations. The experiments demonstrate that, under flow, synchrotron x-ray-diffraction techniques provide a powerful structural probe of steady-state dynamical behavior.

PACS numbers: 61.30.Eb, 64.70.Md, 82.70.Kj

Maxwell and Reynolds realized that the microscopic structure of a fluid should be distorted when $\dot{\gamma}\tau$ becomes comparable to 1.[1] Here, $\dot{\gamma}$ is the shear rate and τ is a relevant relaxation time; in a simple fluid it would correspond to exceedingly fast diffusion times, of order 10^{-12}–10^{-14} s. The required shear rate for observable effects is thus extremely difficult to achieve. In elegant experiments, using large particles to slow down the interparticle diffusion times to about 10^{-2} s, large distortions have been observed at moderate shear rates, in the structure of a fluid of colloidal suspensions.[2] Aside from simple fluid systems where single-particle diffusion sets the time scale, de Gennes and Onuki and Kawasaki were among the early workers to point to the effects of shear flow on pretransitional fluctuations associated with continuous transitions.[3] For these systems, the relevant time scale is the relaxation of a collective fluctuation domain which is readily varied by temperature or pressure, and diverges at the transition.

In this paper, we report on a synchrotron x-ray scattering study of the nematic (N) to smectic-A (Sm-A) phase transition in 4-cyano-4′-octylbiphenyl (8CB), under shear flow conditions. The N-Sm-A transition corresponds to the onset of a one-dimensional mass density wave along the nematic director $\hat{\mathbf{n}}$, a unit vector which specifies the average orientation of the molecules. This transition has been studied extensively at equilibrium primarily because it is a simple example of an almost second-order freezing transition.[4] As the transition is approached in the N phase, the pretransitional Sm-A fluctuation domains, which are directly probed by x rays, grow to length scales of order microns before the Sm-A phase sets in. According to dynamical scaling,[5] the fluctuation relaxation time $\tau \sim \xi^{3/2}$, where ξ is an effective correlation length for critical fluctuations; thus, we chose to study this system because the effective control parameter $\dot{\gamma}\tau$ which drives the system away from equilibrium should increase substantially, near the N-Sm-A transition. We emphasize that our experiments are among the few microscopic studies, probing length scales < 100 Å and as large as $\sim \mu$m, of an ordering transition under nonequilibrium steady-state conditions. Such studies have important bearings on our understanding of phase transitions away from equilibrium and more generally of nonequilibrium statistical-mechanical phenomena.[1-3,6]

The presence of large pretransitional fluctuations in the nematic phase is believed to give rise to a novel *flow-induced-fluctuation force* $\mathbf{h}_f(\dot{\gamma}\tau)$ on $\hat{\mathbf{n}}$.[7,8] We have discovered that in the nematic phase *in situ* standard x-ray-diffraction measurements of the time-averaged distribution of $\hat{\mathbf{n}}$ under flow reveal a sequence of steady-state regimes whose occurrence results from the interplay between the viscous frictional forces and $\mathbf{h}_f$. A very significant finding is that the evolution in the shapes of the x-ray profiles in these regimes allows us to directly observe the renormalization of the shear viscosity α_3, which arises from the critical slowing down of the Sm-A mass-density order-parameter fluctuations, and scales as $\tau/\xi_{\parallel}$, where $\xi_{\parallel}$ is the correlation length along $\hat{\mathbf{n}}$. Thus, the inherently static x-ray tool is probing the dynamics of the system.

We show in Fig. 1(d) the Couette shear cell consisting of two concentric Lexan cylinders with the outer cylinder rotating and the inner one fixed. This approximates a linear velocity profile in the shear plane which contains the velocity ($\mathbf{v}$) and gradient velocity ($\nabla\mathbf{v}$) directions with a constant shear rate $\dot{\gamma} = v/D$, where D is the gap size. Real space is defined in Fig. 1(b), where $\mathbf{v}$ and $\nabla\mathbf{v}$ are along the x and y axes, and the neutral direction parallel to the cylinder axis is along the z axis. In reciprocal space [Fig. 1(c)], $\mathbf{q}_x$, $\mathbf{q}_y$, and $\mathbf{q}_z$ are parallel to $\mathbf{v}$, $\nabla\mathbf{v}$, and the neutral direction. The data showed no significant gap-size dependence for $D = 0.5$, 1.0, and 1.5 mm; here, we present data collected with $D = 1.0$ mm with the inner-cylinder radius fixed at 10 mm. The cell temperature (T) is controlled to within ± 0.005 K. The experiments were primarily carried out at the National Synchrotron Light Source on the Exxon beam line X-10A using 8-keV radiation. The x-ray path was through either the center or the edge of the cell [lines A and B in Fig. 1(d)]. A Braun PSM-50 linear detector placed 95 cm after the sample was positioned as shown in Fig. 1(d)

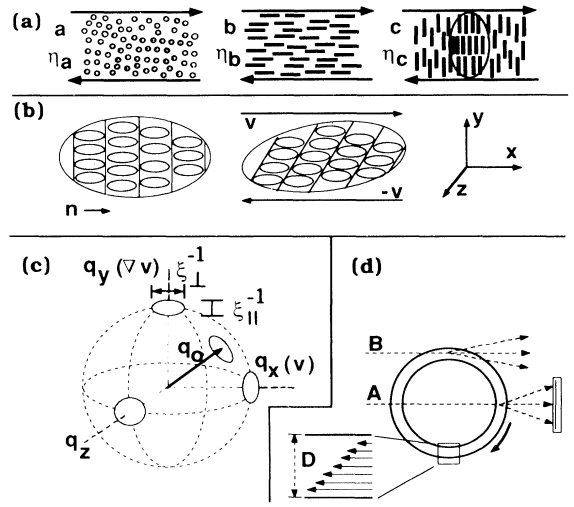

FIG. 1. (a) Three simple orientations for $\hat{\mathbf{n}}$ under shear flow. A Sm-A fluctuation is shown for the c orientation. (b) A Sm-A fluctuation with the b orientation at rest, and under shear which tilts the layers. (c) The a, b, and c orientations would give rise to diffuse scattering spots along q_z, q_x, and q_y in reciprocal space. For a general orientation $\hat{\mathbf{n}}$ (arrow), the spot is also along $\hat{\mathbf{n}}$. (d) Top view of the shear cell showing the two concentric cylinders.

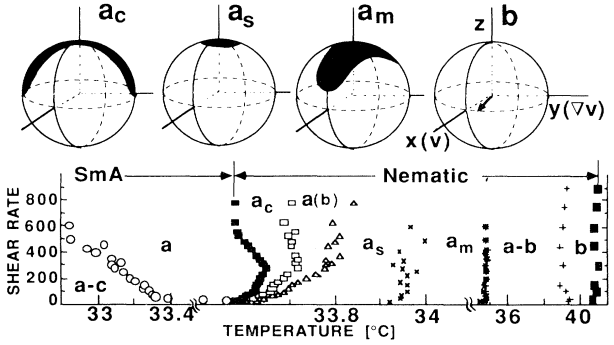

FIG. 2. Bottom: The $\dot{\gamma}$-T phase diagram for 8CB as discussed in the text. Top: Schematics of the stable orientation of $\hat{\mathbf{n}}$ in the b regime (right), and the distribution of $\hat{\mathbf{n}}$ in three of the a regimes.

so that the scattering component collected in the channels was along $\mathbf{q}_x$ ($\mathbf{q}_y$) parallel to $\mathbf{v}$ ($\nabla\mathbf{v}$) when going through the center (edge). The setup gave a $\mathbf{q}_z$ resolution of 3×10^{-4} Å^{-1} (HWHM), with a linear-detector resolution of 1.2×10^{-3} Å (HWHM). The experimental details are described elsewhere.[9]

The three simple orientations that $\hat{\mathbf{n}}$ may assume under flow and their associated viscosities are shown in Fig. 1(a). The a, b, and c orientations refer to $\hat{\mathbf{n}}$ pointing along the neutral $\hat{\mathbf{z}}$, the velocity $\hat{\mathbf{x}}$, and the velocity gradient $\hat{\mathbf{y}}$ directions, respectively. Figures 1(a) and 1(b) show fluctuation domains with anisotropic correlation lengths $\xi_\parallel$ and $\xi_\perp$ and layer spacing d. For a uniform sample with the c orientation where $\hat{\mathbf{n}}=\hat{\mathbf{y}}$, the diffuse x-ray scattering arising from the pretransitional Sm-A fluctuations is centered in reciprocal space at $\mathbf{q}=q_0\hat{\mathbf{n}}=(2\pi/d)\hat{\mathbf{n}}$ along the q_y axis, where the width of the diffuse spot is proportional to $1/\xi_\parallel$ and $1/\xi_\perp$ measured parallel and perpendicular to $\hat{\mathbf{n}}$, respectively [Fig. 1(c)].

The orientational state of $\hat{\mathbf{n}}$ under flow is determined by the total forces acting on it. The Ericksen-Leslie-Parodi (ELP) theory of the hydrodynamics of nematics considers the viscous and elastic torques on $\hat{\mathbf{n}}$.[10] According to ELP nematodynamics, in the high-shear regime where elastic torques are negligible, the viscous torque on $\hat{\mathbf{n}}$ with $\mathbf{v}=\dot{\gamma}y\hat{\mathbf{x}}$ is[10]

$$\Gamma_v=-\hat{\mathbf{n}}\times[\gamma_1\partial\hat{\mathbf{n}}/\partial t+\dot{\gamma}(\alpha_2 n_y,\alpha_3 n_x,0)], \quad (1)$$

where the Ericksen viscosity parameters $\alpha_2=(\gamma_2-\gamma_1)/2$ and $\alpha_3=(\gamma_2+\gamma_1)/2$ are defined in terms of the rotational viscosity γ_1 and shear viscosity γ_2. It follows from Eq. (1) that the viscous torque $\Gamma_v=\dot{\gamma}\alpha_2\hat{\mathbf{z}}$ and $\dot{\gamma}\alpha_3\hat{\mathbf{z}}$ for $\hat{\mathbf{n}}=\hat{\mathbf{y}}$ and $\hat{\mathbf{n}}=\hat{\mathbf{x}}$; thus, α_2 and α_3 are proportional to η_c and η_b, respectively [Fig. 1(a)].

For all nematics studied to date $\alpha_2<0$, and the flow orientation of $\hat{\mathbf{n}}$ depends on the sign of α_3. Normally, far from T_{NA} where fluctuations are negligible, $\alpha_3<0$ with $\alpha_3/\alpha_2\ll1$. The stable solution of the equation of motion (EOM) $\Gamma_v=0$ then results in $\hat{\mathbf{n}}$ lying in the $\mathbf{v}$-$\nabla\mathbf{v}$ shear plane at a small angle $\theta=\tan^{-1}(\alpha_3/\alpha_2)^{1/2}\sim5°$ with the flow direction as we show at the top right of Fig. 2.[11] This is essentially the b orientation of Fig. 1(a). As temperature is reduced towards T_{NA}, the growth of pretransitional Sm-A fluctuations is expected to give rise to a novel flow-induced-fluctuation force $\mathbf{h}_f$ on $\hat{\mathbf{n}}$, which alters the EOM:[7,8]

$$\Gamma_v+\Gamma_f=0, \quad (2)$$

where $\Gamma_f=-\hat{\mathbf{n}}\times\mathbf{h}_f$ is the fluctuation torque on $\hat{\mathbf{n}}$. For $\dot{\gamma}\tau<1$,

$$\mathbf{h}_f=-(\pi/2)(k_BT/d^2\xi_\parallel)(\dot{\gamma}\tau)(\hat{\mathbf{n}}\cdot\hat{\mathbf{v}})\mathbf{y}+O(\dot{\gamma}\tau)^2. \quad (3)$$

We see from Eqs. (1)–(3) that to lowest order in $\dot{\gamma}\tau$ the effect of fluctuations is a renormalization of α_3^R ($\propto\eta_b$):

$$\alpha_3^R=\alpha_3+(\pi/2)(k_BT/d^2)\tau/\xi_\parallel. \quad (4)$$

The physical origin of $\mathbf{h}_f$ is due to the effect of shear flow on the fluctuation domains. Figure 1(b) shows that for a temporal fluctuation domain with $\hat{\mathbf{n}}=\hat{\mathbf{x}}$ pointing along $\mathbf{v}$ in the b orientation shear flow tends to tilt the layers, which changes the layer spacing and gives rise to the restoring force $\mathbf{h}_f$. In contrast, shear flow does not alter the internal structure of fluctuations with the a and c orientations.

When $\alpha_3^R>0$, there is no stable solution in the shear plane. However, there is a zero-torque solution if $\hat{\mathbf{n}}$ points exactly along the neutral $\hat{\mathbf{z}}$ direction; this is the a orientation of Fig. 1(a). Therefore, the fluctuation-corrected ELP nematodynamics predicts that as T is lowered, $\hat{\mathbf{n}}$ should exhibit a flip transition from a b state when $\alpha_3<0$ to an a state when $\alpha_3^R>0$ [Fig. 1(a)]. Pre-

vious optical experiments have found that the sign change in α_3^R occurs in 8CB at $T \approx T_{NA} + 5.5\,^\circ\mathrm{C}$.[11] The emphasis in our work is in the behavior of $\hat{\mathbf{n}}$ in the immediate vicinity of T_{NA}, where $\dot{\gamma}\tau$ becomes of order 1 and α_3^R is expected to diverge. In this limit with $\alpha_3^R (\gg |\alpha_3|) > 0$, Eq. (2) reduces to lowest order in n_x, n_y, and $\dot{\gamma}\tau$, to

$$\partial^2 n_x/\partial t^2 + \omega_0^2 n_x = 0\,, \tag{5a}$$

$$n_y = (-\gamma_1/\alpha_2\dot{\gamma})\partial n_x/\partial t\,, \tag{5b}$$

where we consider deviations of $\hat{\mathbf{n}} = (n_x, n_y, 1)$ away from the z axis, and $\omega_0^2 = \dot{\gamma}^2(-\alpha_2\alpha_3^R)/\gamma_1^2$. Equation (5) describes a coupled-harmonic-oscillator motion for n_x and n_y with precession frequency ω_0. The coupling of the precession modes, which are of the form $n_x(t) = n_{x0}\cos(\omega_0 t)$ and $n_y(t) = n_{y0}\sin(\omega_0 t)$, describe an equation of an ellipse:

$$n_x(t)^2/n_{x0}^2 + n_y(t)^2/n_{y0}^2 = 1\,. \tag{6}$$

Thus, the EOM describes an anisotropic precession of $\hat{\mathbf{n}}$ on a unit sphere about the z axis, where the projection of $\hat{\mathbf{n}}$ onto the x-y plane will be *elliptical* with a well-defined ratio of axes $n_{x0}/n_{y0} = (-\alpha_2/\alpha_3^R)^{1/2}$. We expect that the precession of $\hat{\mathbf{n}}(t)$ about $\hat{\mathbf{z}}$ should be accompanied by wanderings, due to thermal or hydrodynamic noise, between different amplitude states n_{x0} and n_{y0}, but with a ratio of amplitudes n_{x0}/n_{y0} fixed by temperature. Therefore, the distribution of $\hat{\mathbf{n}}$ about $\hat{\mathbf{z}}$ would also be anisotropic with an elliptical projection on the x-y plane with eccentricity n_{x0}/n_{y0}, which we expect to be strongly temperature dependent due to the critical behavior of α_3^R near T_{NA}. This is precisely what we find near T_{NA} as we now discuss.

We show in Fig. 2 the $\dot{\gamma}$-T phase diagram with emphasis on the distinct narrow regimes in the immediate vicinity of T_{NA}. The solid squares indicate thermodynamic transitions from the isotropic to the N phase ($T_{IN} \approx 41\,^\circ\mathrm{C}$), and from the N to the Sm-A phase ($T_{NA} = 33.58\,^\circ\mathrm{C}$ at $\dot{\gamma} = 10\ \mathrm{s}^{-1}$), which shows an unexpected reentrant behavior. In the Sm-A phase, $\hat{\mathbf{n}}$ assumes the a orientation but at lower temperature crosses into a regime where Sm-A domains with both the a and c orientations coexist. Over a 2° range below T_{IN}, we find that $\hat{\mathbf{n}}$ lies in the shear plane in the b orientation with the diffuse scattering centered at $\mathbf{q} \sim q_0\hat{\mathbf{x}}$. This stable orientation for $\hat{\mathbf{n}}$ is shown schematically at the top right of Fig. 2. As we further lower T, $\hat{\mathbf{n}}$ undergoes a flip transition, through an intermediate regime labeled a-b in Fig. 2, to a region near T_{NA} where the average orientation of $\hat{\mathbf{n}}$ is along $\hat{\mathbf{z}}$. However, this nominally a regime where $\alpha_3^R > 0$ consists of four crossover regimes a_m, a_s, $a(b)$, and a_c. The shaded areas covering the unit spheres at the top of Fig. 2 are schematics of the distribution of $\hat{\mathbf{n}}$ for three of these regimes.

These four regimes exhibit distinct x-ray scattering profiles. For an arbitrary orientation of $\hat{\mathbf{n}}$, the diffuse spot is at $\mathbf{q} = q_0\hat{\mathbf{n}}$ in reciprocal space as we show in Fig. 1(c); thus, because the peak q-vector *points* along $\hat{\mathbf{n}}$, one is able to measure its orientation. For an anisotropic (or isotropic) distribution of $\hat{\mathbf{n}}$ about the z axis, the diffuse scattering would now be on a corresponding anisotropic (or isotropic) "patch" of a sphere of radius q_0 centered about the q_z axis. To elucidate the orientational distribution of $\hat{\mathbf{n}}$, we plot in Figs. 3(b)–3(e) equal-intensity contours at $\dot{\gamma} = 300\ \mathrm{s}^{-1}$ of cuts in the three planes q_z-q_x, q_z-q_y, and q_x-q_y through the point $(0,0,q_z = q_0)$, at one reduced temperature $t = (T - T_{NA})/T_{NA}$ in each of the four regimes [a_m, a_s, $a(b)$, and a_c]. In our description, we emphasis the overall shapes of the contours. *In particular, the elliptically shaped intensity distributions in the q_x-q_y shear plane (Fig. 3, left column) which result from an anisotropic distribution of $\hat{\mathbf{n}}$ about the z axis are self-evident.* We see clearly that the shapes evolve

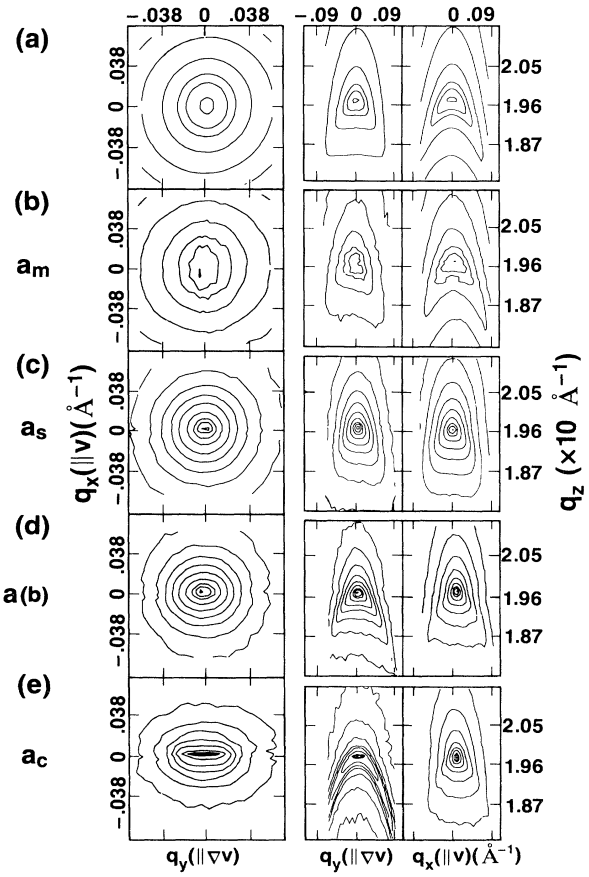

FIG. 3. (b)–(e) Equal-intensity contours of the x-ray intensity in the q_x-q_y, q_z-q_y, and q_z-q_x planes through $(0,0,q_z = q_0)$, in four a regimes at $\dot{\gamma} = 300\ \mathrm{s}^{-1}$. The intensity levels normalized to the peak (central dots) fall off as $1 : \frac{7}{8} : \frac{3}{4} : \frac{1}{2} : \frac{1}{4} : \frac{1}{8} : \frac{1}{16} : \frac{1}{32} : \frac{1}{64} : \frac{1}{128}$. The data are for decreasing $T \to T_{NA}$: (b) $t = 0.0035$, (c) 0.000 82, (d) 0.000 26, and (e) 0.000 05. The evolution in the shapes of the contours is due to the divergence of the viscosity α_3^R arising from the critical slowing down of the order-parameter fluctuations. (a) Result of fit of the data of (b) with $I(\mathbf{q})$ as discussed in the text.

as a function of decreasing temperature. In the a_m regime the elliptical distribution in the q_x-q_y shear plane has its major axis along $q_x(\|\mathbf{v})$ with $n_{x0}/n_{y0}>1$, which would correspond to the range where $\alpha_3^R<-\alpha_2$; this is consistent with the anisotropic distribution in the other two planes which is more spread out in the q_z-q_x plane indicating larger deviations of $\hat{\mathbf{n}}$ towards the $\mathbf{v}$ direction as compared to the $\nabla\mathbf{v}$ direction. With increasing α_3^R, the elliptical shapes of Fig. 3 (left column) are first squashed into an almost circular shape in the a_s regime where $n_{x0}/n_{y0}\approx 1$ which indicates that $\alpha_3^R\approx-\alpha_2$, and then become elliptical again in the $a(b)$ regime, but now with the major axis along $q_y(\|\nabla\mathbf{v})$ with $n_{x0}/n_{y0}<1$ because $\alpha_3^R>-\alpha_2$. This is consistent with cuts in the other two planes in Figs. 3(c) and 3(d) (center and right), where the distribution of $\hat{\mathbf{n}}$ becomes confined to a narrow isotropic cone about the q_z axis in the a_s regime, and slightly anisotropic again in the $a(b)$ regime with larger deviations in the q_z-q_y plane. Finally, the elliptical contour of Fig. 3(e), left column, exhibits extreme anisotropy in the a_c regime where $\alpha_3^R\gg-\alpha_2$, and the contour lines in the q_z-q_y plane extend to the q_y axis [Fig. 3(e), center]. The distribution of $\hat{\mathbf{n}}$ about $\hat{\mathbf{z}}$ now extends down to the $\nabla\mathbf{v}$ direction as we show in the top left of Fig. 2. Thus, *the evolution in the anisotropic x-ray profiles in the vicinity of the nematic to Sm-A phase transition allows us to directly observe the divergence of the viscosity ratio* $\alpha_3^R/\alpha_2\sim\tau/\xi_\|$, *arising from the critical slowing down of the Sm-A order-parameter fluctuations.*

An important observation of the data is found in comparing the distribution of $\hat{\mathbf{n}}$ in the q_z-q_x plane in the four regimes [Figs. 3(b)–3(e), right]. As one lowers temperature from the a_m to the other regimes, the large excursions of $\hat{\mathbf{n}}$ away from the z axis become confined to the z-∇v plane. This results from the next term of order $(\dot\gamma\tau)^2$: $-0.13(k_BT/d^2\xi_\|)(\dot\gamma\tau)^2(\hat{\mathbf{n}}\cdot\hat{\mathbf{v}})\hat{\mathbf{x}}$ in the expansion of $\mathbf{h}_f$ [Eq. (3)], which adds a frictional damping term $(1/\tau_N)\partial n_x/\partial t$ to the EOM of Eq. (5),[8] and produces a fluctuation-induced normal torque on $\hat{\mathbf{n}}$ pushing it towards the z-∇v plane. We expect this higher-order term to lead to overdamped motion of $\hat{\mathbf{n}}$ about $\hat{\mathbf{z}}$ with $\tau_N^{-1}>\omega_0$, only for $T-T_{NA}\le 1$ mK, where $\dot\gamma\tau$ approaches 1. We have labeled the a regimes a_m for marginally stable where the damping term is negligible, a_s for stable (the normal torque confines $\hat{\mathbf{n}}$ to the z-∇v plane), a_c where the anisotropic precession of $\hat{\mathbf{n}}$ about the z axis extends down to the y axis parallel to the c orientation of Fig. 1(a), and $a(b)$ since some intensity reappears in the shear plane at $\mathbf{q}\sim q_0\hat{\mathbf{x}}$ which corresponds to the b orientation of Fig. 1(a).

To estimate the growth in the ratio α_3^R/α_2, we chose a sensible functional form for the orientational distribution function averaged over time and the sample volume: $\langle W(\hat{\mathbf{n}})\rangle\propto\exp[-(n_x^2\sigma_x^2+n_y^2\sigma_y^2)]$ with $\sigma_x/\sigma_y=n_{x0}/n_{y0}=(-\alpha_2/\alpha_3)^{1/2}$. The x-ray intensity

$$I(\mathbf{q})\propto\int\int dn_x\,dn_y\langle W(\hat{\mathbf{n}})\rangle S(\mathbf{q},\hat{\mathbf{n}}),$$

where $S(\mathbf{q},\hat{\mathbf{n}})$ is the diffuse scattering due to pretransitional Sm-A fluctuations.[12] We show contour plots in Fig. 3(a) which are a result of a nonlinear-least-squares fit of the data of Fig. 3(b) with $I(\mathbf{q})$, which qualitatively reproduce our data. Over the nominal a regimes which span a reduced temperature range of $4\times10^{-3}<t<5\times10^{-5}$, $\alpha_3^R/|\alpha_2|=(n_{y0}/n_{x0})^2$ varies by a factor of $\sim$70. In 8CB, $|\alpha_2|\approx 3$ P (Ref. 11) independent of T; thus, over the same temperature range, we estimate from Eq. (4) that the fluctuation relaxation time $\tau\approx(2/\pi)\alpha_3^R\times\xi_\|d^2/k_BT$ grows between ~1 μs for $t=4\times10^{-3}$ and $\sim10^3$ μs for $t=5\times10^{-5}$.

To measure α_3^R and $\tau(\xi,\dot\gamma)$ quantitatively, the distribution function has to be obtained numerically from the full nonlinear EOM of Eq. (2) and compared to the data.[9] This would allow for a detailed test of dynamical scaling for this one-dimensional freezing transition, and the nature of its breakdown as the transition is pushed further away from equilibrium at very-high-shear rates. More generally, these synchrotron-based x-ray-diffraction experiments open up the possibilities for structural studies of nonequilibrium systems under steady-state conditions.

We acknowledge useful discussions with Jacques Prost, Tom Lubensky, and Shobo Bhattacharya. One of us (C.R.S.) is especially grateful to Robijn Bruinsma for many stimulating conversations. The National Synchrotron Light Source is supported by DOE.

[1]J. C. Maxwell, Proc. Roy. Soc. London **148**, 46 (1873); O. Reynolds, Philos. Mag. **20**, 469 (1885).

[2]N. A. Clark and B. J. Ackerson, Phys. Rev. Lett. **44**, 1005 (1980).

[3]P. G. de Gennes, Mol. Cryst. Liq. Cryst. **34**, 91 (1976); A. Onuki and K. Kawasaki, Ann. Phys. (N.Y.) **121**, 456 (1979).

[4]J. D. Litster and R. J. Birgeneau, Phys. Today **35** (5), 26 (1982); P. S. Pershan, *Structure of Liquid Crystal Phases* (World Scientific, Singapore, 1988).

[5]P. C. Hohenberg and B. I. Halperin, Rev. Mod. Phys. **49**, 435 (1977).

[6]D. Beysens, M. Gbadamassi, and L. Boyer, Phys. Rev. Lett. **43**, 1253 (1979); Y. C. Chou and W. I. Goldburg, Phys. Rev. Lett. **47**, 1155 (1981).

[7]W. L. McMillan, Phys. Rev. A **9**, 1720 (1974); F. Janig and F. Brochard, J. Phys. (Paris) **35**, 301 (1974).

[8]R. F. Bruinsma and C. R. Safinya, Phys. Rev. A (to be published).

[9]C. R. Safinya, E. B. Sirota, R. J. Plano, R. Bruinsma, and C. Jeppesen (to be published).

[10]J. L. Ericksen, Arch. Ration. Mech. Anal. **4**, 231 (1960); F. M. Leslie, Quart. J. Mech. Appl. Math. **19**, 357 (1966); O. Parodi, J. Phys. (Paris) **31**, 581 (1970).

[11]P. Pieranski and E. Guyon, Phys. Rev. Lett. **32**, 924 (1974); K. Skarp *et al.*, Mol. Cryst. Liq. Cryst. **66**, 199 (1981).

[12]Note that $S(\mathbf{q},\hat{\mathbf{n}})=a\xi_\|^2/[1+\xi_\|^2(\hat{\mathbf{n}}\cdot\mathbf{q}-q_0)^2+\xi_\perp^2(\hat{\mathbf{n}}\times\mathbf{q})^2+d\xi_\perp^4(\hat{\mathbf{n}}\times\mathbf{q})^4]$; see Ref. 4.